# $\alpha$ Spectroscopy

Sara Fiorendi - Riccardo Manzoni - Monica Tarantino
2007/2008

**Abstract**

Our experiment consist in $\alpha$ spectroscopy measures, using solid state silicon detectors. Our radioactive sources will be $^{241}Am$ and Uranium minerals.After a brief experimental apparatus characterisation, including a *dead layer* valuation, we then proceed with $\alpha$-matter interaction (Range and Bragg curves), followed by $\alpha$ radioactivity measurements. We then finish our experience reproducing Rutherford experiment.

# 1 Experimental apparatus

The experimental apparatus we have used basically consists in:


- a spectrometer for $\alpha$ spectroscopy, provided with a silicon surface barrier detector (preferred to drifted silicon detectors because of their thinner dead layer). There are two power options: *bias*, used for normal data taking with a radioactive source into the spectrometer chamber, and *pulse*, used during the preliminary phase of the experiment to calibrate the entire apparatus, without any source into the chamber. The voltage can be varied through an adjustable resistance situated at the back of the spectrometer. In the source chamber it is also possible to create vacuum to the pressure of *32 mbar*;
- a preamplifier, which integrates the charge deposited in the detector, and in such way generates a current signal;
- an amplifier and a shaper, which give a specific temporal shape to the signal and purify it from electronic noise;
- an ADC and an MCA, which acquire the analogic signal and convert it into digital, sending it through a specific channel so to transfer the information to a PC. The Computer then uses a specific software called *Maestro* to plot such signals.

The software used for data analysis is *Root*[1].

# 2 Detector characterisation

For our purposes, we will make use of two different detectors, one of $50\text{mm}^2$ and one of $900\text{mm}^2$. First thing to do before using the spectrometer is to find its best operating conditions, studying its response when we vary external parameters such as incident particles energy or bias voltage.

[1] http://root.cern.ch/

We are firstly going to study its response to voltage adjustments. As we said, it is possible to vary bias voltage manually; let us misure the output signal (called *dark current*) as a function of bias voltage, misured at the ends of a known resistance of 1.1 MΩ. As the trend is not linear, we use a fit function of the form:

$$I(V) = aV^b + cV^d \tag{1}$$

obtaining the following results:

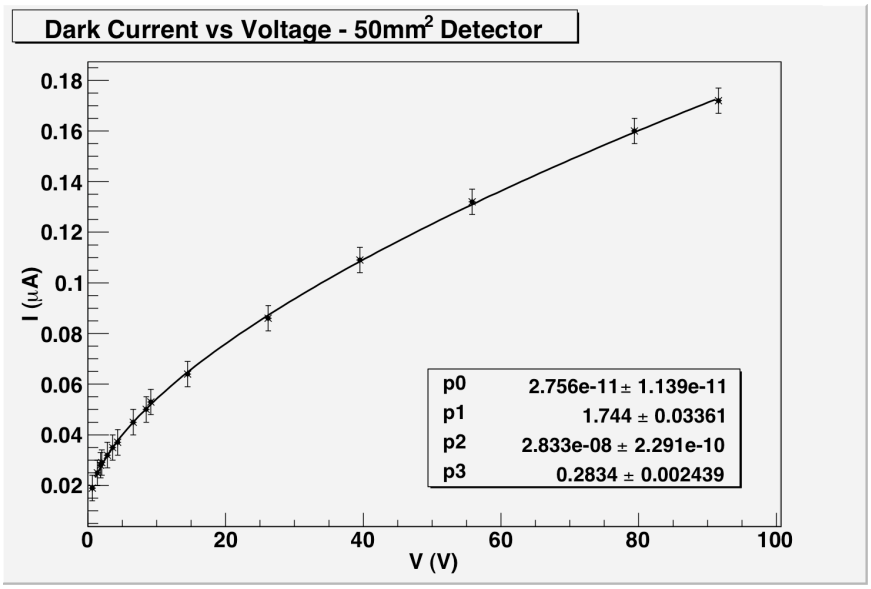


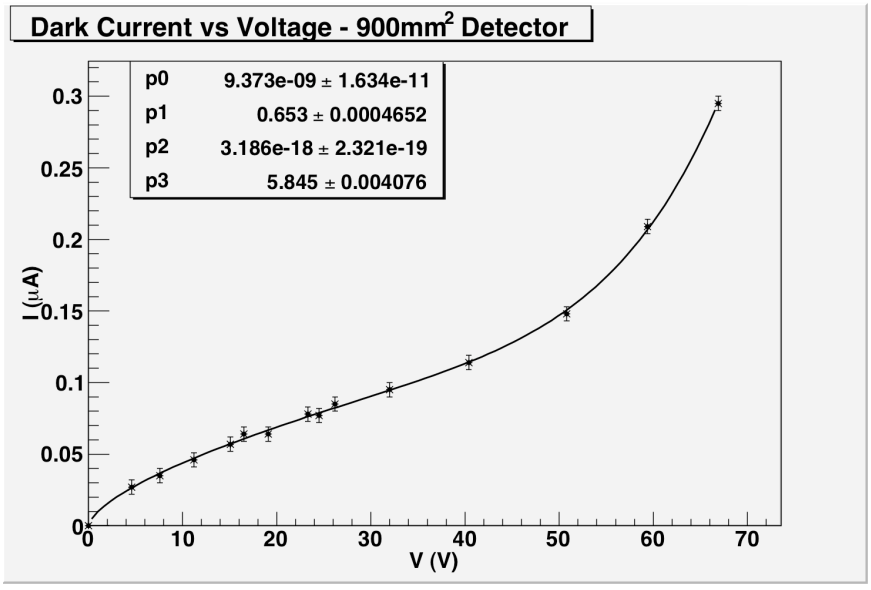

Let us now study what happens if we vary the pulser energy instead of the bias voltage. In an ideal situation we would expect that, sending to the detector a monoenergetic beam, the signal is always converted into the same channel, and thinking of representing on a plot the counts distribution $\frac{dn}{dE}$, this would result in a very sharp peak centered on $E_0$. Actually, the detector cannot measure with infinite precision, so we define its resolution as

$$R = \frac{FWHM}{E_0} \tag{2}$$

There are two main indipendent reasons for the resolution worsening:

- signal noise, which can have different origins, one due to the detector capacity, and the other one due to the escape current inside the *p-n* junction (caused by secondary charge carriers);
- shot noise, that consists of random fluctuations of the electric current inside the *p-n* junction, which are caused by the fact that the current is carried by discrete charges. If the events that liberate charge carriers are indipendent from one another, the entire process is described by a Poisson distribution (with a small correction called the *Fano factor*), but for a number $n$ of charge carriers $\geq 20$ it can be approximated with a Gaussian distribution. Let $N$ be the mean value of the liberated charge carriers, then we have:

$$\sigma \propto \sqrt{N} \tag{3}$$

$$\frac{FWHM_{stat}}{N} = 2.35\frac{\sigma}{N} = 2.35\frac{1}{\sqrt{N}} \tag{4}$$

  and knowing that $E \propto N$ we have that this statistical process affects the detector resolution with a term proportional to $\frac{1}{\sqrt{E}}$.

Indeed, it is possible to isolate the two contributes singularly. If we send a pulse to the detector without any source in the chamber, we can study noise production by the electronic components, and see how this can affect the *FWHM.* With the pulser energy ranging from 1 to 8 MeV, we obtain various peaks, fitting each one with a gaussian curve to obtain their *FWHM* and their position. Drawing *FWHM vs* energy (E) we got the following plots:

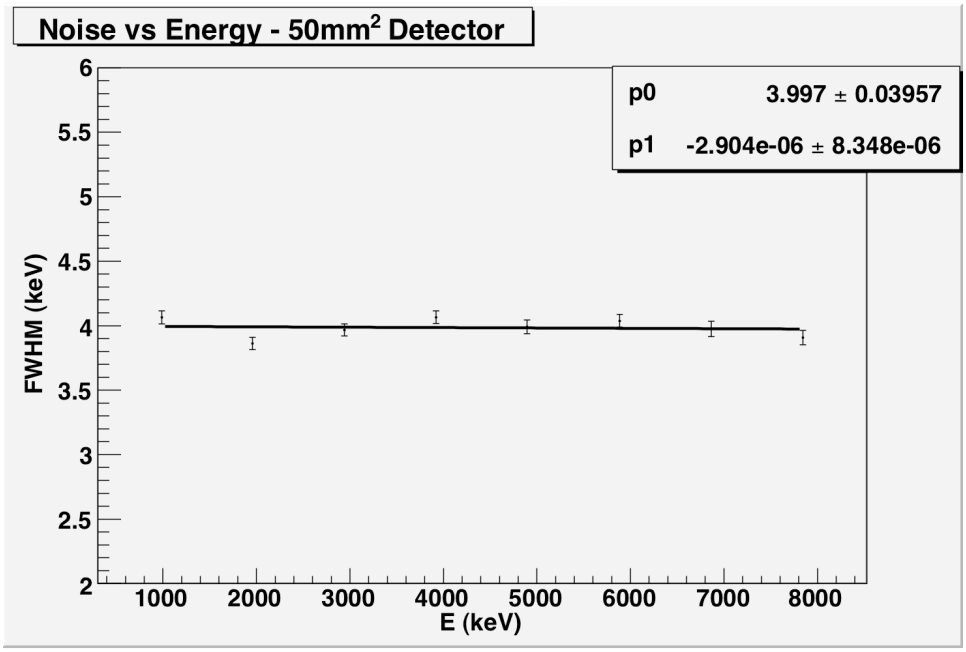


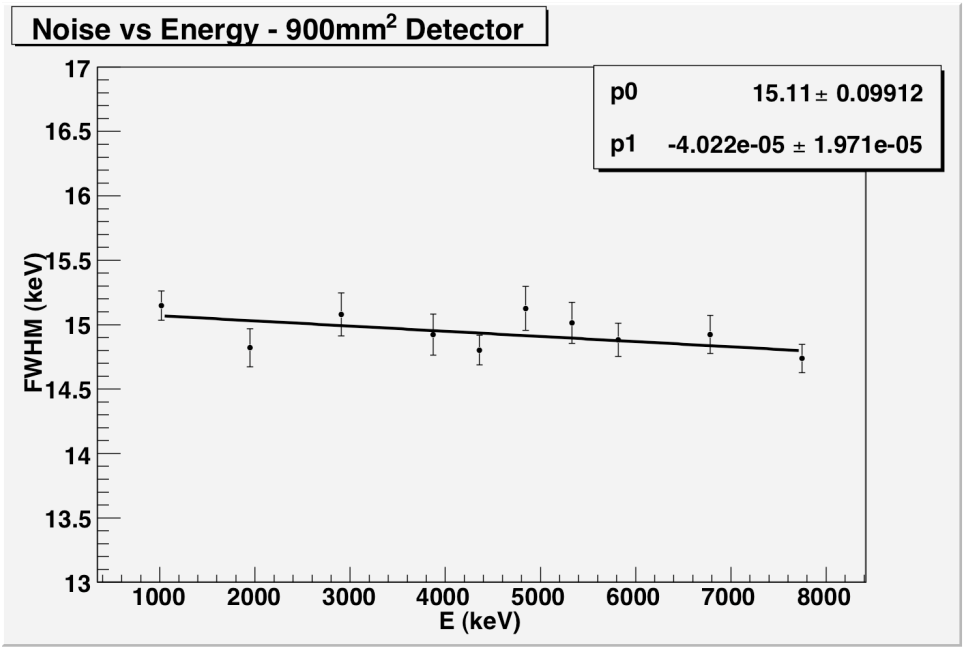


$FWHM_{50}$=4,00±0,04 keV

$FWHM_{900}$=15,11±0,10 keV.

Let us now plot the peaks positions *vs* energy, instead, and we obtain the two detectors calibration curves. They are very useful, seen that the histograms we get from the

PC have the $x$-axis in channels, and we need to know the calibration to convert them into energies.

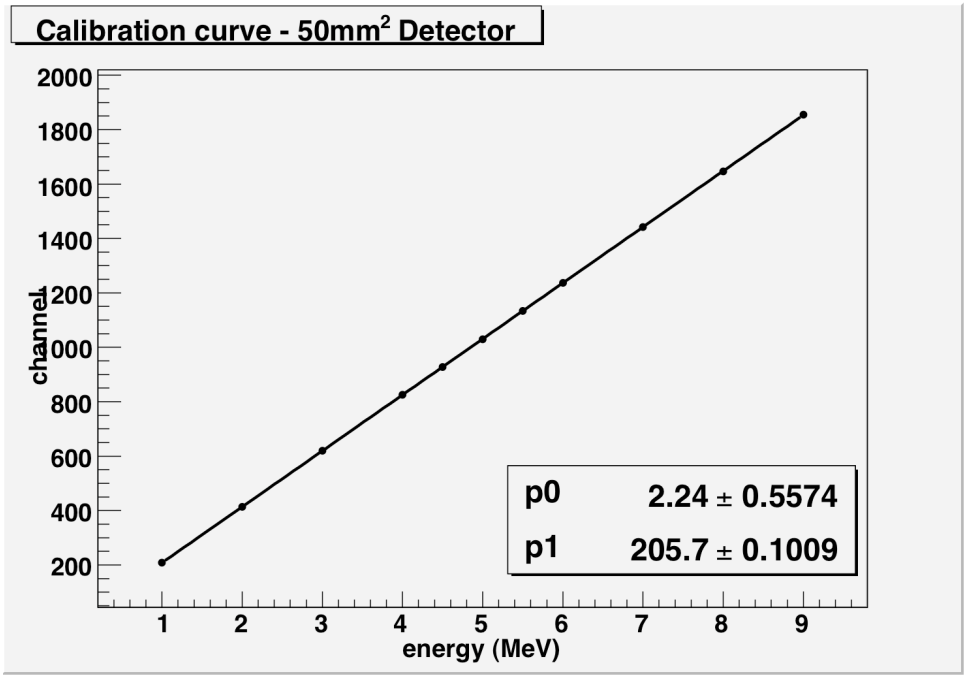


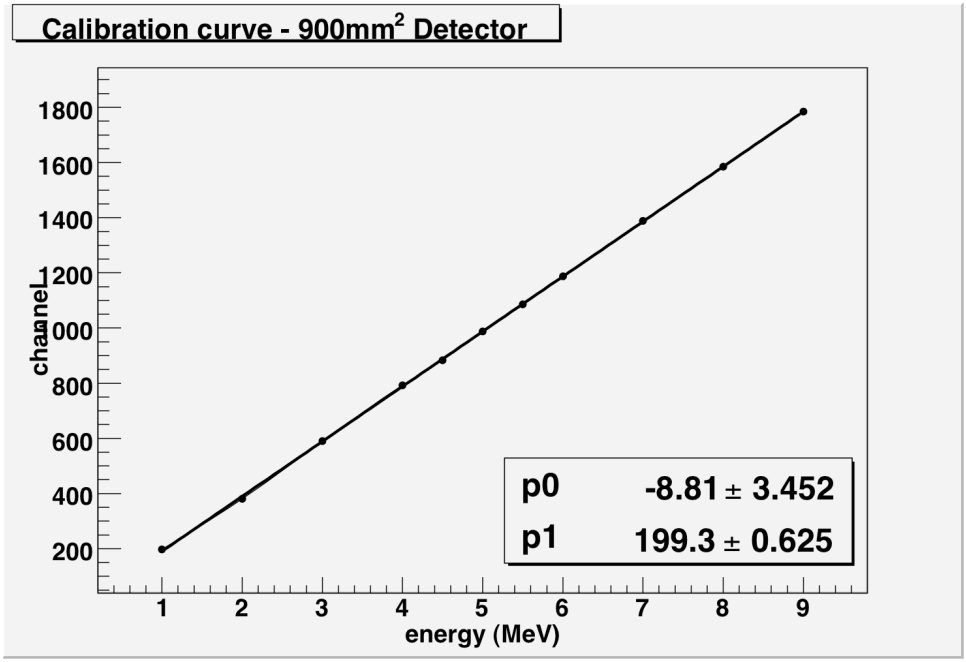


We can also calculate the *Equivalent Noise Charge*, or *ENC*, which is the minimum

charge we can detect, given a background noise. The *ENC* is defined as

$$ENC = \left[ a\frac{C^2(V)}{\tau} + bI(V)\tau \right]^{\frac{1}{2}} \tag{5}$$

where C(V) is the detector internal capacity:

$$C(V) = \varepsilon\frac{S}{d} \propto \frac{1}{\sqrt{V}} \tag{6}$$

and $\tau$ the measurement duration (about $10s$). To measure the *ENC*, we vary bias voltage given a fixed pulser energy and, proceeding as before, we then fit the resulting peaks to get their *FWHM*. Using a function like (5) to fit, and replacing I(V) with the values given from (1), we obtain:

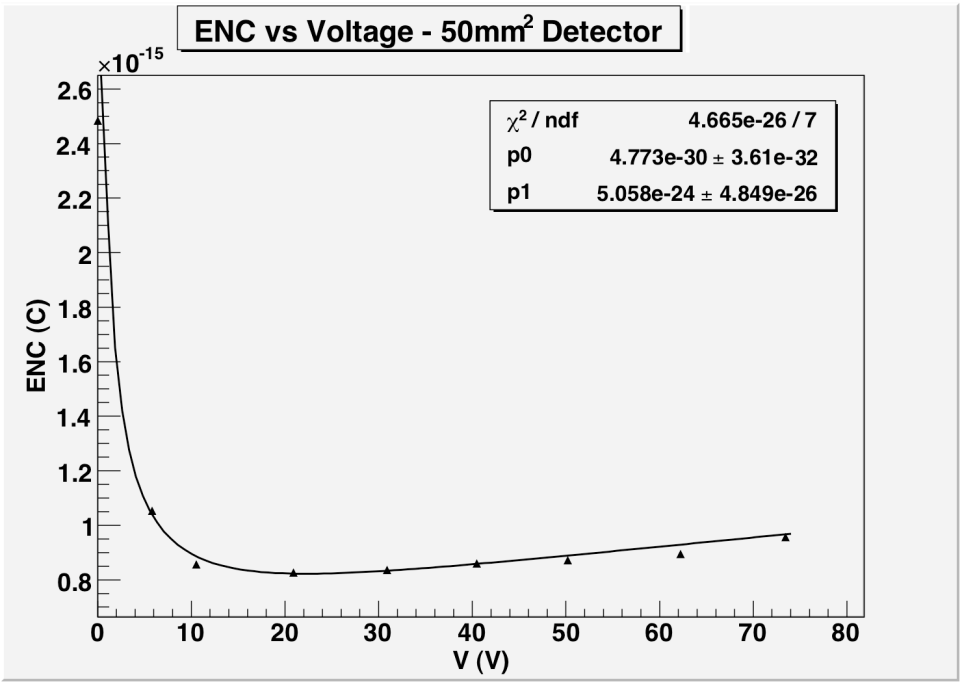

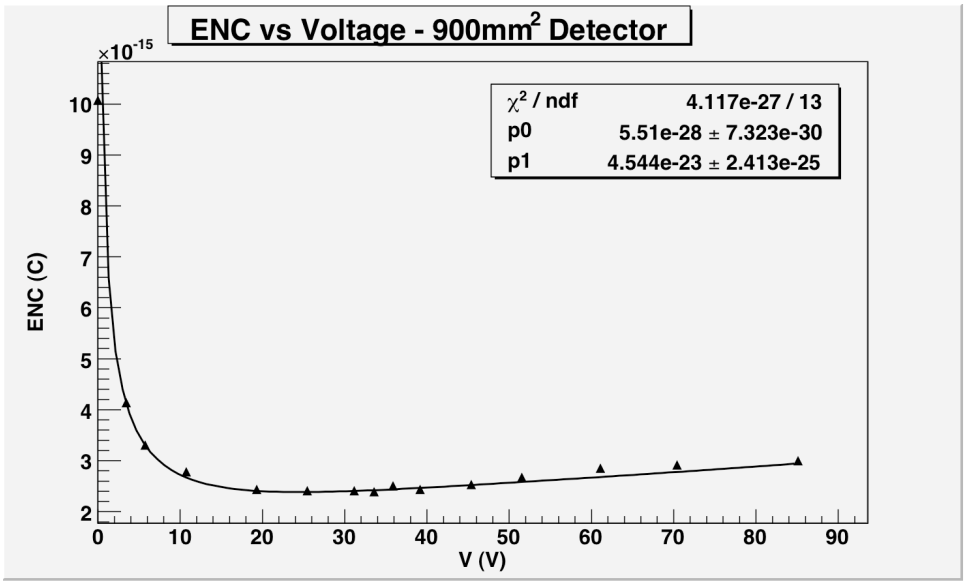


The first term, which depends on the detector capacity, is proportional to $\frac{1}{V}$, and so prevails for small voltages; as for voltages over 50V the current increases notably, therefore it is not appropriate to power instruments at higher voltages.

From the plots we have obtained we can note that the best bias voltage, for which we have minimum noise, is between 20V and 40V for the 50mm$^2$ detector, as for the 900mm$^2$ one it is slightly more, we find it is between 30V and 50V.

## 2.1 Energy calibration using Uranium mineral

In order to get a definite calibration indipendent of a possible pulser offset we use a known source, in this case Uranium mineral. Indeed Uranium daughters elements are not detectable until Radon because of the presence of a paper filter that stops $\alpha$ particles from $U$ decay. $Rn$, a subproduct of the decay chain, is a gas, and therefore can spread and fill the chamber. The detected spectrum will show only lines from $Rn$ and its daughters.

The well known $^{222}Rn$, $^{219}Rn$, $^{218}Po$, $^{214}Po$, $^{211}Bi$ $\alpha$ decay spectrum[2] is compared with the measured one, and the corrispondence between these spectra yields the channel-energy calibration relation.

Here the measured spectra from both detectors and respective calibrations are shown.

$$E = 4.850 * channel - 56.50$$

$900mm^2$ detector calibration

$$E = 4.766 * channel - 19.35$$

$50mm^2$ detector calibration

[2]data from *http://atom.kaeri.re.kr/*

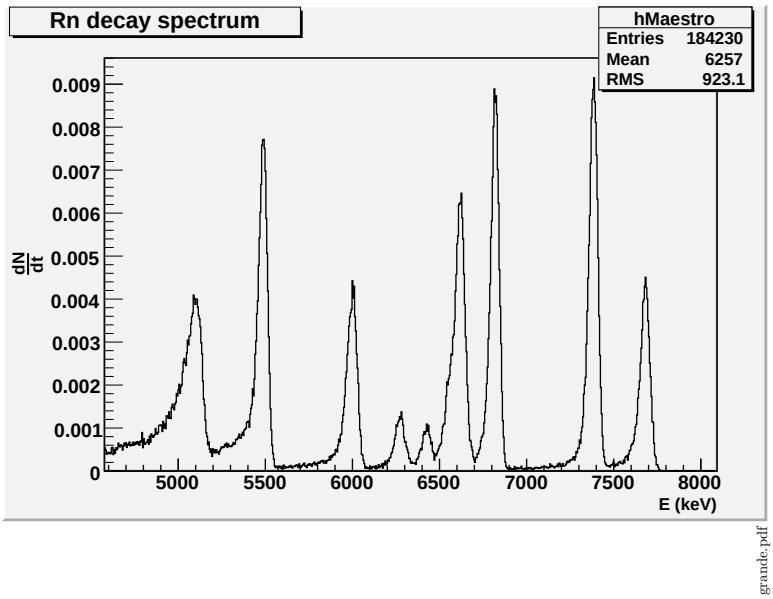


Figure 1: $900mm^2$ detector

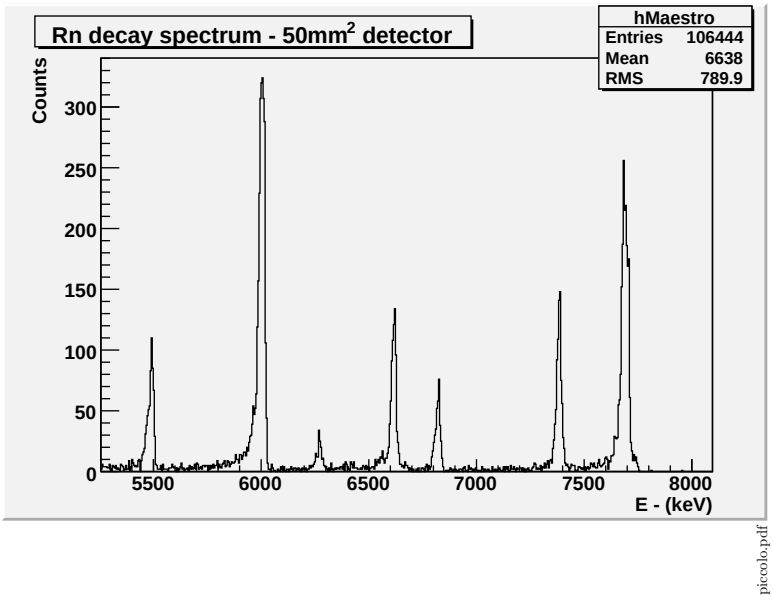


Figure 2: $50mm^2$ detector

# 3 $^{241}Am$ Spectrum

During different experiences a $^{241}Am$ source has been used. Here its spectral analysis is reported.

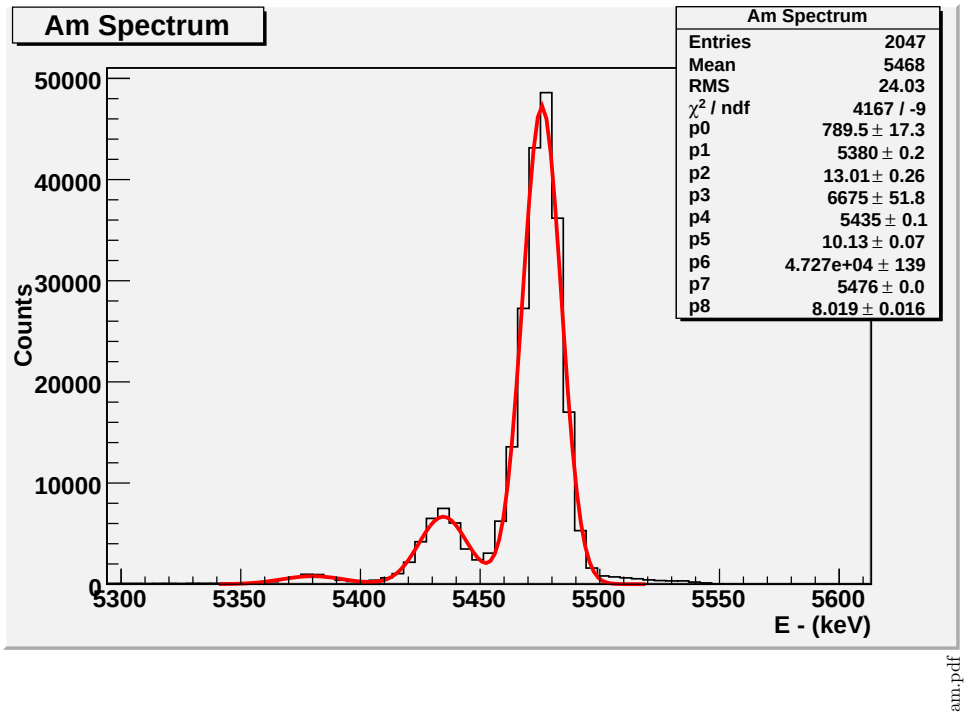


We are expecting three different peaks separated by approximately $40keV$, so the $50mm^2$ detector is required because of its greater resolution ($FWHM = 4keV$); in fact the $900mm^2$ detector cannot resolve the three peaks because of its $FWHM = 15,11keV$.

| $E_{measured}(keV)$ | $E_{expected}(keV)$ | $\Delta E(keV)$ | $B.R._{measured}$ | $B.R._{expected}$ |
|---|---|---|---|---|
| 5476 | 5485 | 9 | 84,2 % | 84,5 % |
| 5435 | 5443 | 8 | 14,0 % | 13,0 % |
| 5380 | 5388 | 8 | 2,1 % | 1,6 % |

Expected intensities are in good agreement with our measures, while peaks energies are understimated by $\sim 8,5keV$. This discrepancy is to be reconducted to the energy loss in air, valuable from *Bragg curve*; in these pressure conditions equivalent path is remarkably small and so it is possible to assume constant $\frac{dE}{dx} \cong 800keV/cm$. From these assumptions we get $E_{lost} \cong 9keV$, that makes our measure very close to the tabulated one.

# 4 Dead layer

Typical of semiconductor detectors is a dead layer where particles lose part of their energy.
Its thickness can be evaluated by changing the incidence angle of the particles emitted from the source: this way the dead layer area that is passed through, and consequently the energy lost in this region, depends on the cosine of the incidence angle, following the relation:

$$E_{\alpha,meas} + E_{lost} = E_{\alpha,0} - \frac{\Delta E}{cos\theta}$$

where $E_{lost}$ is the energy lost in air and $\Delta E$ the energy lost passing through the dead layer. The measured energy of incident $\alpha$ has to be corrected considering the energy loss during the path in air.

The correction is evaluated from the $\frac{dE}{dx}$ value we got from Bragg curve and adapting it for a pressure of 28 *mbar*.

Since this value would bring to $E_\alpha + E_{lost} > E_{\alpha,0}$ we come to the conclusion that the pressure value (that is directly proportional to the equivalent range in air) is overestimated. We therefore apply a systematic correction to $E_{lost}$. Error on source position is small compared to uncertainty on peak identification and on pressure measurement and for this reason is neglected.

The *dead layer* thickness $t$ is obtained through a line that fits the corrected points: from $p_1$ parameter and the known value for Silicon of $\frac{dE}{dx}$ ($\frac{dE}{dx} = 135.5 keV/\mu m$) we get a measure of $t$ from the relation

$$t = \frac{p_1}{135.5} \frac{keV}{keV/\mu m}$$

The $p_0$ parameter represents the original energy of $\alpha$, that is the peak energy of $^{241}Am$

## 4.1 $900 mm^2$ detector

At the beginning of this experiment, a plastic mask is placed on the detector, leaving uncovered an outer circle of radius $r = 1.1 cm$ and width 0.12 cm. The $^{241}Am$ source is approximated to a point source thanks to a disc with a centred hole of radius 0,15 cm and it is placed on the bottom of the chamber (the initial detector-source distance is 3.35 cm) under the center of the detector. In order to change the incidence angle of the particles the source is raised 0,4 cm every measurement, up to a minimum distance of 0,8 cm.

$$t = 0,176 \pm 0,036 \mu m$$

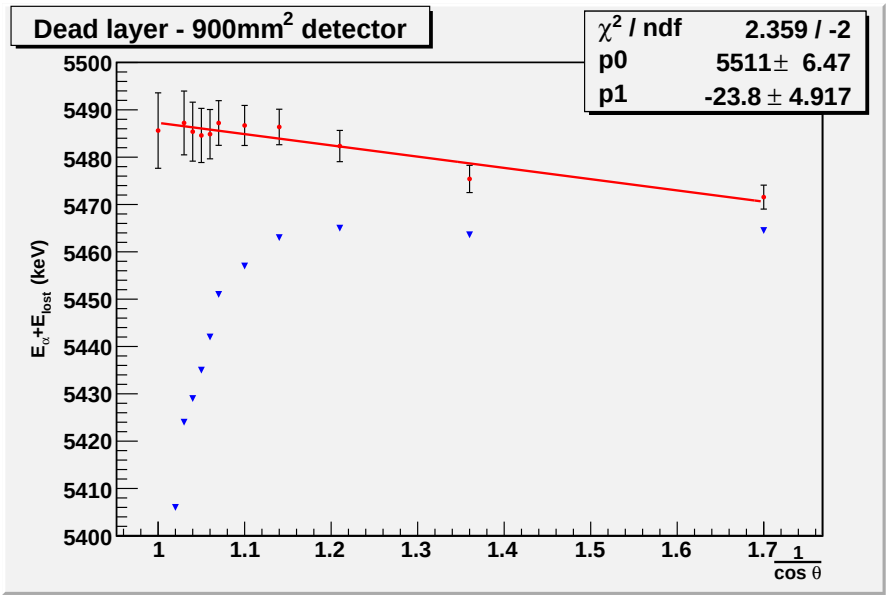


## 4.2 $50mm^2$ detector

In this case, as we are not provided with a smaller plastic mask for the $50mm^2$ detector, we made a paper mask with a hole in the center of approximately 0.16 cm diameter, while the source, screened as in the previous case, is placed in a corner of the chamber. The initial distance of 3.6 cm is reduced every run by 0.4 cm up to a minimum distance of 1.6 cm. Uncertainties have been estimated as in the previous case.

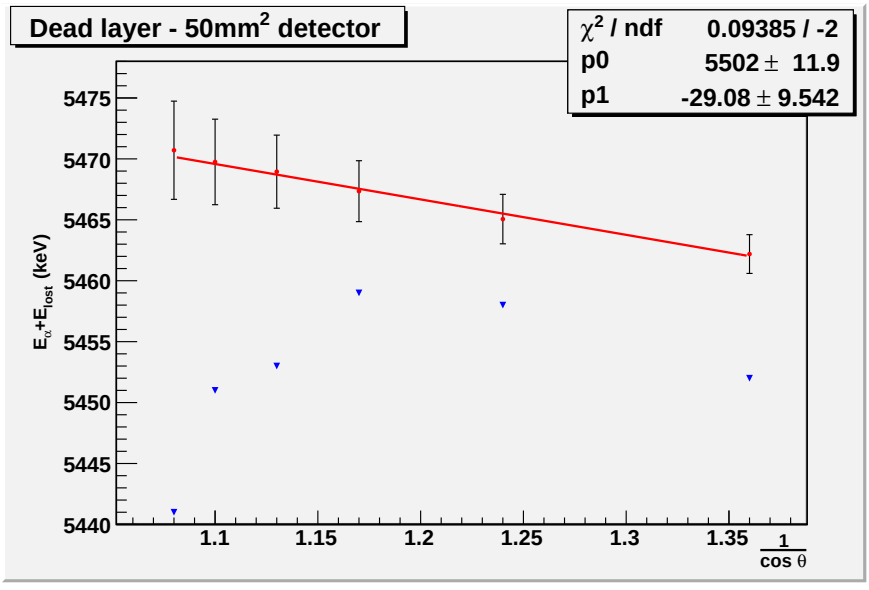


$$t = 0,213 \pm 0,070 \mu m$$

# 5 Range and Bragg curve

The purpose of this experience is to determine the Range curve and the Bragg curve. The first one describes $\alpha$ interaction with matter by showing the maximum range and the seconde curve describes the energy loss for path covered. $^{241}Am$ source is used (precisely its strongest line ($E_\alpha = 5,485MeV$)) and $50mm^2$ detector because a great resolution is required in measuring $\Delta E$ for high-pressure close-to-zero conditions.

We can notice that the $^{241}Am$ spectrum loses its shape since the beginning, when pressure is low, due to line widening, and we cannot resolve the secondary peaks from the main one. We take as measured energy the mean value of this distribution. A change in the equivalent path lenght is obtained through pressure control in the chamber; in fact we have that

$$x_{eq} = \frac{p \cdot h \cdot T_0}{p_0 \cdot T}$$

where $h$ is the real path covered, $T_0 = 293,15K$ and $p_0 = 1013,25mbar$ are the standard temperature and pressure conditions and $p$ and $T$ represent pressure and temperature in the chamber. The pressure data are taken from a voltmeter with sensitivity of $0,005V$; the relation between voltage and pressure is supposed to be linear and since the atmospherical pressure corresponds to $5V$ and imposing that V=0⇒ P=0 we get the following equation:

$$p(mbar) = \frac{p_0(mbar)}{5000mV} \cdot V(mV)$$

Uncertainty is given by measure fluctuations as well as voltmeter precision, in any case larger than $10mV$ ($2mbar$).

## 5.1 Range curve

We can now draw in a graph counts number normalized to $I/I_0$ versus the equivalent path lenght $x_{eq}$. $I_0$ is the mean value of the intensity of the first counts, since we expect that there is no loss in intensity in the first part of the path. Errors valuation takes into consideration the poissonian nature of counts (independent and unrelated events $\sigma_N = \sqrt{N}$) and the uncertainty in pressure measure.

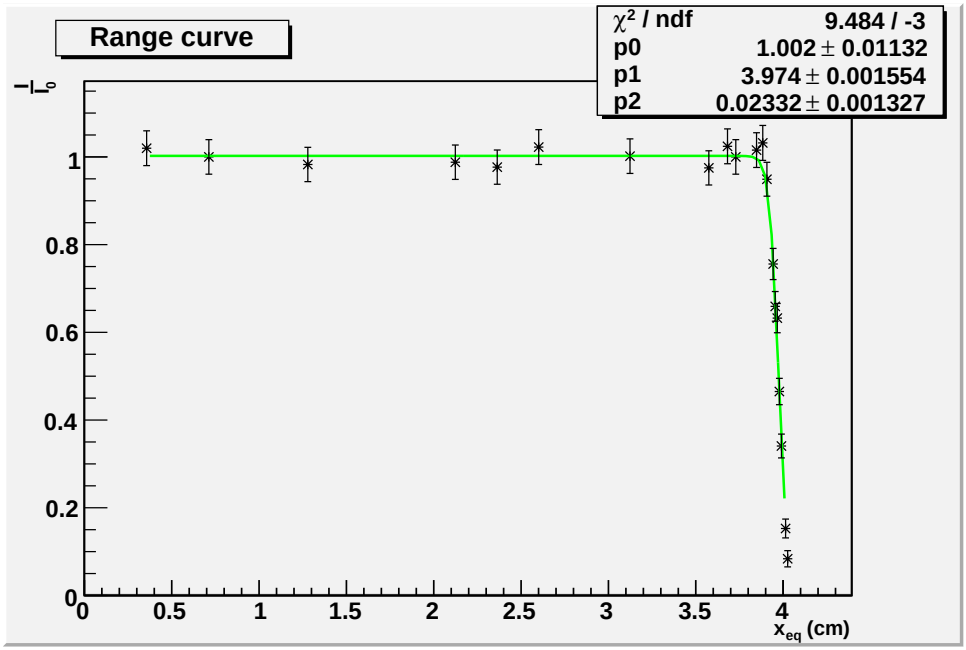


A Fermi function fits the data:

$$\frac{I}{I_0} = \frac{p_0}{1 + exp((x - p_1)/p_2)}$$

and we get an estimate of the range value

$$R_m = (3,9741 \pm 0,0016)cm \qquad R_{est} = (4,0554 \pm 0,0042)cm \qquad straggling = (0,0813 \pm 0,0058)cm$$

where $R_m$ is the range value at $I/I_0 = 0.5$ (mean range) and $R_{est}$ is the range extrapolated at the point of the curve maximum pendence.

## 5.2 Bragg curve

The Bragg curve is the plot of $dE/dx_{eq}$ versus $x_{eq}$; basically we have calculated the ratio $\Delta E/\Delta x$ (where $\Delta E$ is the difference between the mean energies of two consecutive measurements) for $x$ intervals small enough. Error valuation takes into account uncertainties both on energy determination and on pressure measure, and weights more on end-of-range measurements.

The graph also shows the expected curve that has been built from data[3] referring to Bethe-Bloch curve $\frac{dE}{d\rho x}$ versus $E_\alpha$. To obtain Bragg curve we have to go back to the equivalent path integrating

[3] reported on http://physics.nist.gov/PhysRefData/Star/Text/ASTAR.html

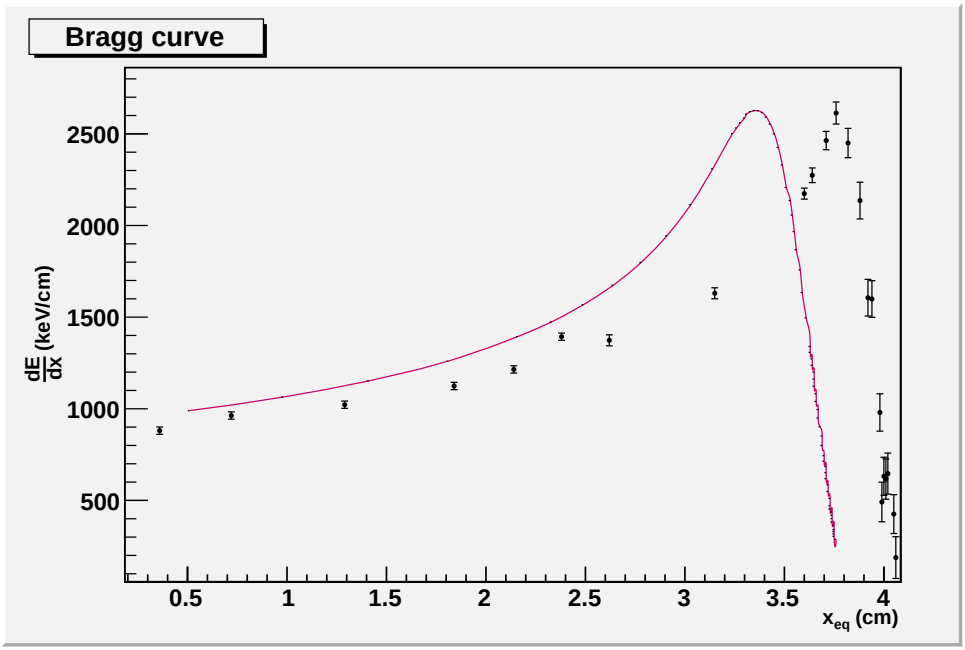


$$x_{eq} = \int_0^{E_\alpha} \frac{\rho dx}{dE} dE$$

Practically, having discrete data, the integral reduces to the sum:

$$x_n = \sum_{i=1}^{n} \left( \frac{\rho dx}{dE} \right)_i \Delta E_i$$

Finally we have to normalize the x and y axis, multiplying by $\rho_{air}$. We can get the stopping power of air using the first part of the range:

$$\frac{dE}{dx} \cong 800 keV/cm$$

This datum is needed in order to evaluate the energy lost in air by $\alpha$ particles in *dead layer* measurements and in Americium spectrum. The discrepancy between the measured curve and the expected one leads to the hypothesis that voltage-pressure calibration is not correct, and particularly there is a systematic pressure overestimation. This hypothesis is in good agreement with the correction to the $E_{lost}$ in *dead layer* measurements. We think that the correction we have to apply to pressure measures is systematic because our curve is shifted from the expected one of a fixed and predictable amount.

# 6 Alpha radioactivity measurements

During this experiment, we will study $\alpha$ emission from minerals containing uranium. The experimental set-up is simple: in the chamber, the source is placed inside an open-top cylindrical box, facing the $50\text{mm}^2$ detector. This detector will allow us to have sharper peaks, easier to recognize, although we will have a smaller active area compared to the $900\text{mm}^2$ one.

A pump will also be connected to the chamber, to create (or mantain) vacuum if needed. We will indeed perform the measurements with two different set-ups: the first time, switching the pump on to evacuate the chamber, and then turning it off; the second time we will leave the pump on during the whole data taking process. This change in external conditions will affect the most the activity of two Radon isotopes, $^{222}Rn$ and $^{219}Rn$, and their daughter radionuclides. In fact, Radon is a gas, and being volatile it can be sucked up by the pump (in case it is on), therefore changing the conditions inside the chamber. Equilibrium is then reached (if at all) at different stages.

The data taking for such an experiment requires a long time. However, we have automated the procedure programming the software *Maestro* to save the data every $1800s$ in a different file, resetting the previous measurements once done so, and opening a new file every time. This way we obtain several files which, once summed up, allow us to have the whole spectrum, and taken singularly, they allow us to monitor the mineral activity every half an hour, opening the files one by one.

## 6.1 Emission spectra

The following graphs are the mineral emission spectra, in both pump on/off cases.

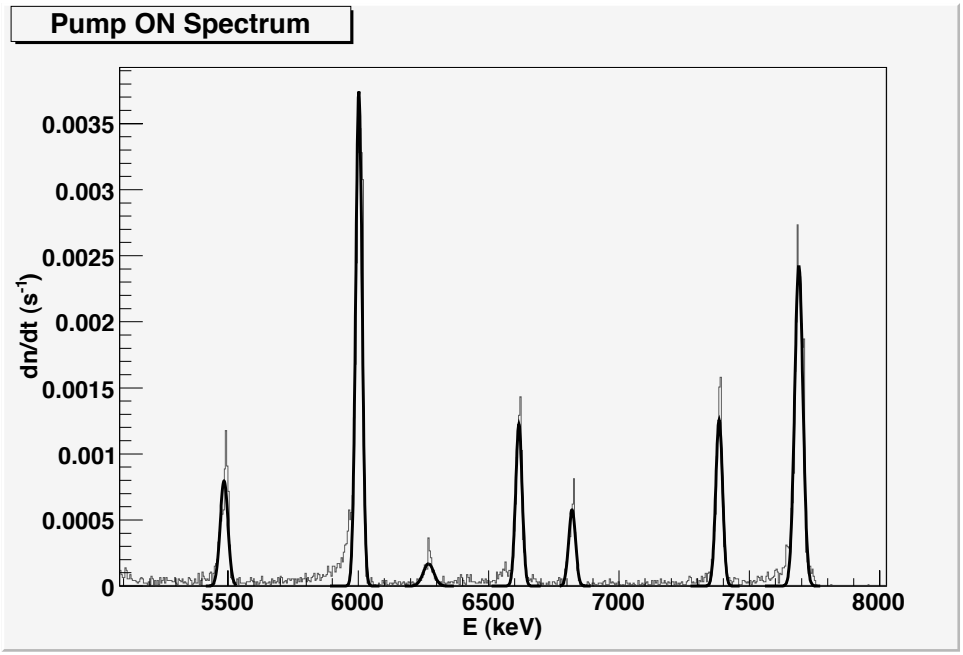

For the "pump on" case, the spectrometer has been left measuring for about $93600s$, and the resulting spectrum has got extremely sharp peaks which, as one can see from the graph, have been fitted with Gaussian curves to obtain their position with high precision, allowing us to recognize the source element.

These are the results:

| Element | $E_{tabulated}$[4] $(keV)$ | $E_{measure}$ $(keV)$ | $\Delta E$ $(keV)$ |
|---|---|---|---|
| $^{222}Rn$ | 5489 | 5484 | -2 |
| $^{218}Po$ | 6002 | 6001 | -1 |
| $^{211}Bi$ | 6278 | 6269 | -9 |
| $^{219}Rn$ | 6425 | n/a | n/a |
| $^{219}Rn$ | 6553 | n/a | n/a |
| $^{211}Bi$ | 6623 | 6615 | -8 |
| $^{219}Rn$ | 6819 | 6819 | 0 |
| $^{215}Po$ | 7386 | 7383 | -3 |
| $^{214}Po$ | 7687 | 7689 | 2 |

For the "pump off" case, the spectrometer has been left measuring for about $417600s$. In this case, it is more difficult to recognize with precision the peaks, because they are not as sharp as before, as the pressure inside the chamber rises of several $mbar$. In fact, with the pump off, at the beginning the pressure settles around $32mbar$, but does not stay like that for the whole time (the chamber door is not complitely airtight, although we did apply some vacuum grease). Gradually, this slow rising results in more energy loss by the $\alpha$ particles before they reach the detector, and so the peaks slowly shift on the left (towards lower energies), and they show marked tails mostly due to particles emitted futher away from the detector (hence losing more energy).

This trend is explicitly showed in the second graph, where data have been divided into four parts and plotted in four different histograms, each one reporting counts registered during a time span of $6960s$. We can note that from the first histogram (in black) to the last one (in lightest gray), the peaks did not only shifted, but they have widened as well.

The peaks analysis in this case is the following:

| Element | $E_{tabulated}$ $(keV)$ | $E_{measured}$ $(keV)$ | $\Delta E$ $(keV)$ |
|---|---|---|---|
| $^{222}Rn$ | 5489 | 5451 | -35 |
| $^{218}Po$ | 6002 | 5994 | -8 |
| $^{211}Bi$ | 6278 | 6215 | -63 |
| $^{219}Rn$ | 6425 | n/a | n/a |
| $^{219}Rn$ | 6553 | n/a | n/a |
| $^{211}Bi$ | 6623 | 6585 | -38 |
| $^{219}Rn$ | 6819 | 6758 | -61 |
| $^{215}Po$ | 7386 | 7350 | -36 |
| $^{214}Po$ | 7687 | 7639 | -48 |

It is clear that, due to the widening and shifting movement of the whole spectrum

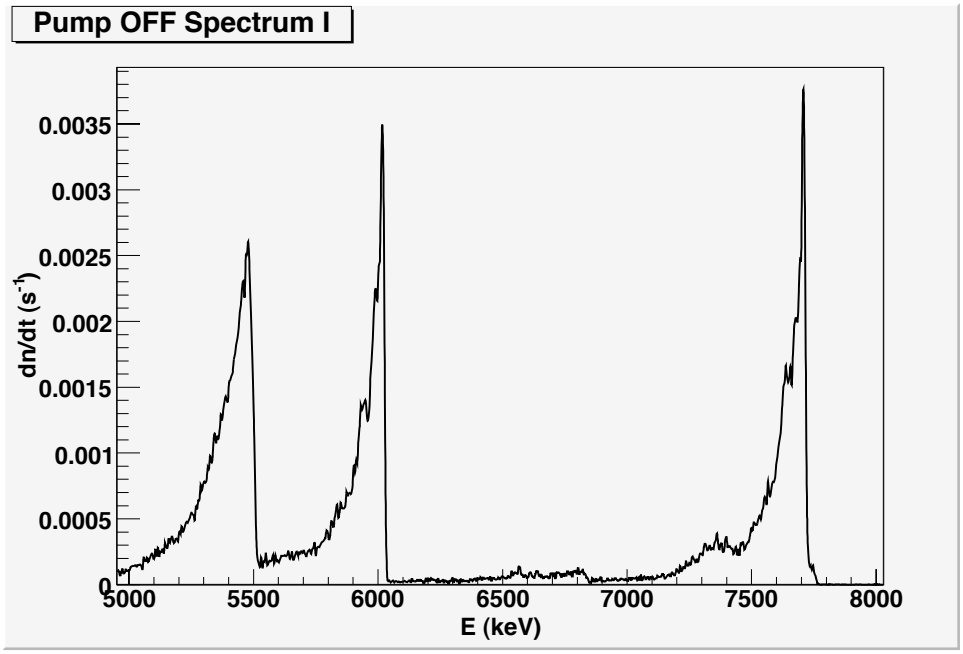


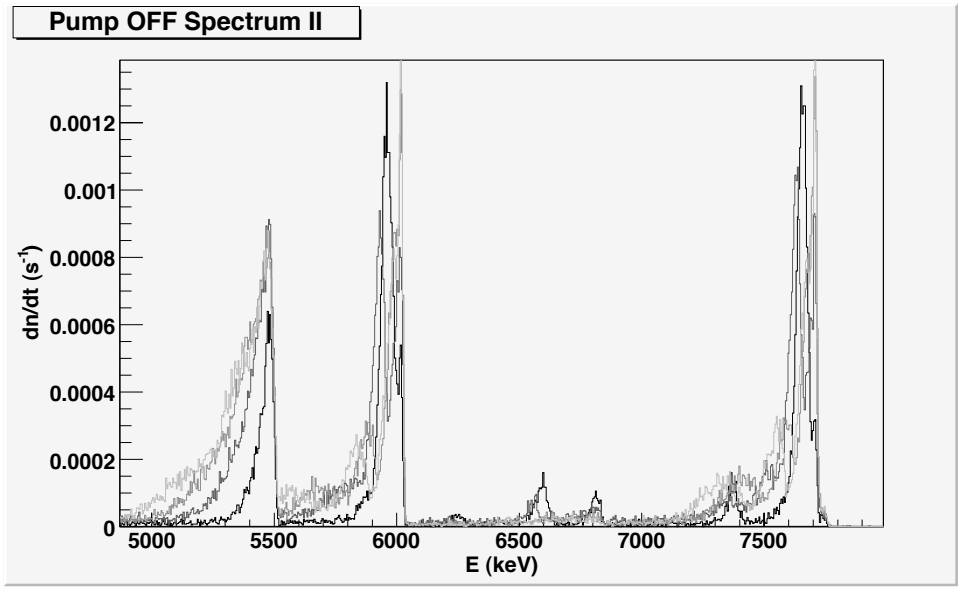


as time passes, in this case the differences between $E_{measured}$ and $E_{tabulated}$ are much stronger than the previous ones. Nevertheless, the spectrum is clearly recognizable.

Finally, let us draw on the same plot the two emission spectra to compare them directly (in full line the "pump on" spectrum, in dashed line the "pump off" one), using for the y-axis the counting rate to normalize the two data sets:

First thing to point out is the drastic reduction of the $^{222}Rn$-peak from the pump-on spectrum to the pump-off one, as most of the gas cannot decay before being sucked out

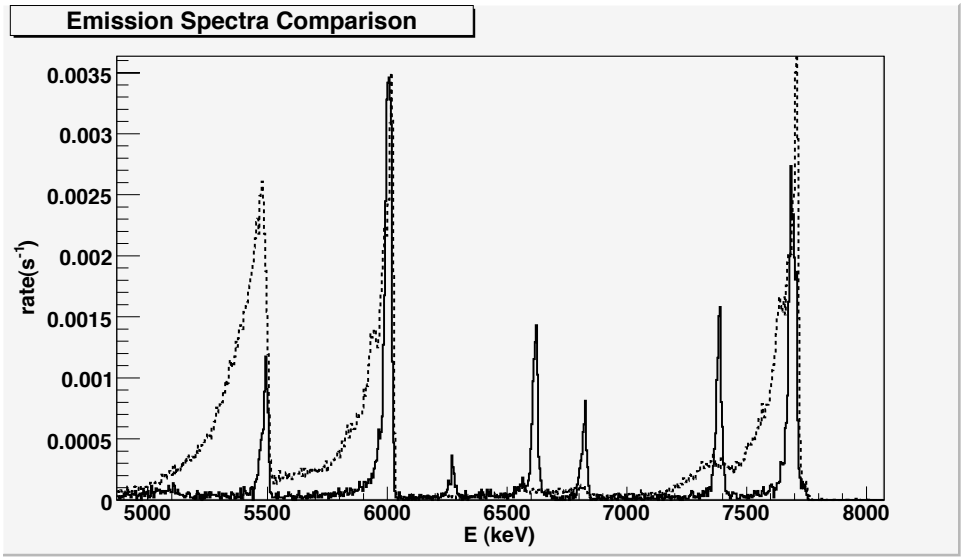


the chamber (as its half-life is around 3.82 days), and this obviously affects the daughter activities too ($^{214}Po$ and $^{218}Po$ peaks). As for $^{219}Rn$, the same thing does not happen, because this isotope has a much shorter half-life ($3.96s$), hence it is not affected by the pump sucking.

### 6.1.1 Experimental Note

During the data taking for this analysis, we happened to notice that, performing a measurement even without any source in the chamber, one could still notice some counts in proximity of $^{214}Po$. This happens because, despite the fact that the mineral itself is not inside the chamber, both the chamber and the detector have been contaminated by $^{222}Rn$ daughters, that keep on decaying ($\alpha$ and $\beta$) following the $^{238}U$ decay chain:

$^{222}Rn$ ($\alpha$) $\rightarrow^{218}Po$ ($\alpha$, $3.1min$) $\rightarrow^{214}$ $Pb$ ($\beta$, $26.8min$) $\rightarrow^{214}$ $Bi$ ($\beta$, $19.9min$) $\rightarrow^{214}$ $Po$ ($\alpha$, $164\mu s$)

In order to get a clean environment, it is necessary to wait for some time (at least a few hours) for the background to die out, hence not influencing the following measurements.

This background radioactivity can as well be seen from the fact that in the pump-off spectrum, both Polonium peaks show a splitting in the form of a smaller peak on the left side of the bigger one; this is caused by the radionuclides on the chamber walls that keep on decaying. The same does not happen during the pump-on measurements because Radon is in great part sucked out, therefore the chamber is kept cleaner.

## 6.2 On $^{222}Rn$ activity

Our study is mainly based on the well known decay law:

$$\frac{dN}{dt} = -\lambda N(t) \tag{7}$$

In our case though it is necessary to add a term that accounts for the fact that a certain amount of nuclei is constantly introduced inside the chamber, coming from the $^{238}U$ and $^{235}U$ decays inside the mineral. We shall name the term $v$, which for $^{222}Rn$ is obviously proportional to $^{238}U$ activity:

$$v(^{222}Rn) \propto \lambda(^{238}U)N(^{238}U) \tag{8}$$

$$\frac{dN}{dt} = -\lambda N(t) + v \tag{9}$$

Depending on the set-up configurations, sometimes it will be appropriate to add further terms to eq.(9) to describe the situation properly.

When the pump is switched on, for istance, we have to consider that a part of $^{222}Rn$ is sucked out before it can decay; we shall add to eq.(9) a term that takes it into account, and we shall consider this term proportional to the number of nuclei inside the chamber at that given time. Eq.(9) then becomes:

$$\frac{dN}{dt} = -\lambda N(t) + v - kN(t) \tag{10}$$

its solution is

$$N(t) = \frac{v}{\lambda + k}(1 - e^{-(\lambda+k)t}) \tag{11}$$

Activity is therefore

$$\lambda N(t) = \frac{\lambda v}{\lambda + k}(1 - e^{-(\lambda+k)t}) \tag{12}$$

Fitting the $^{222}Rn$ activity data using a function of the form of eq.(12), we obtain:

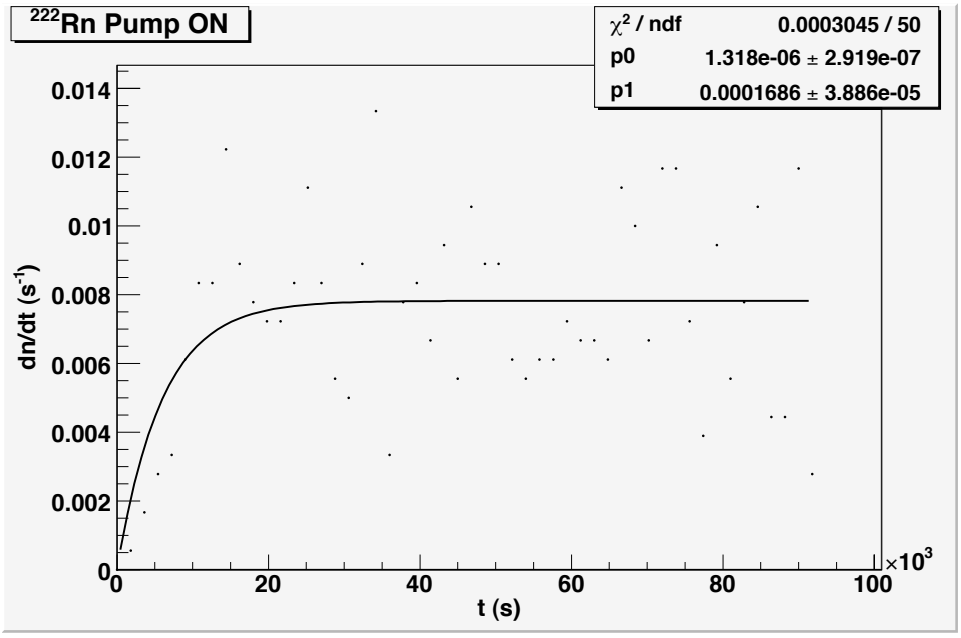


In case of pump switched off, instead, eq.(9) already describes fully the situation. In this case, activity is defined by:

$$\lambda N(t) = v(1 - e^{-\lambda t}) \tag{13}$$

Fitting with this equation our data regarding pump-off measurements, we obtain:

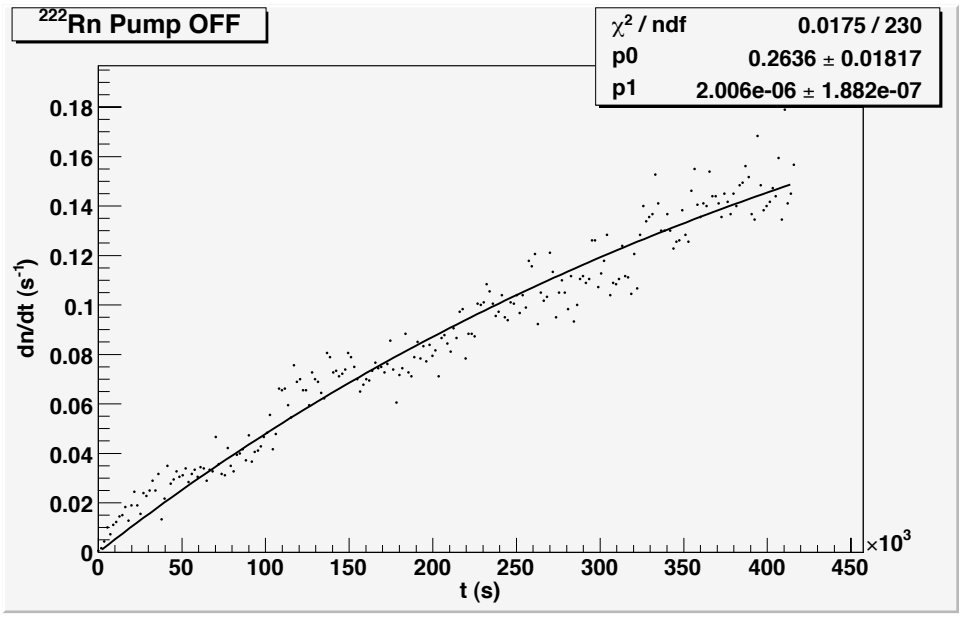

It is possible to calculate $^{222}Rn$ half-life from the fit parameters. Parameter *p1* is indeed the decay constant $\lambda$, and using the formula

$$\tau_{\frac{1}{2}} = \frac{log2}{\lambda} \tag{14}$$

we obtain

$$\boxed{\tau_{\frac{1}{2}}(^{222}Rn) = (4.00 \pm 0.37)\,d}$$

which is in good agreement with the tabulated value of $3.82\,d$.

## 6.3 On $^{219}Rn$ activity

$^{219}Rn$ has an half-life a lot shorter compared to the one of $^{222}Rn$, $\tau_{\frac{1}{2}}(^{219}Rn) = 3.96s$ compared to $\tau_{\frac{1}{2}}(^{222}Rn) = 3.82d$, and so the differences between the two different set-ups are not as clear, as only a small part of undecayed $^{219}Rn$ is sucked out. Thanks to this short decay time, equilibrium is soon settled, as we can note from the activity plots:

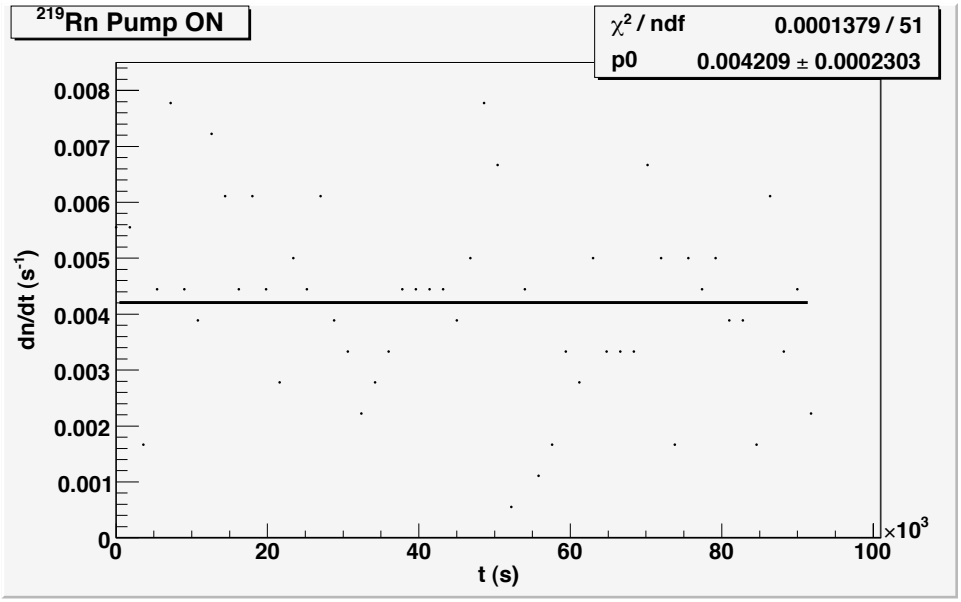

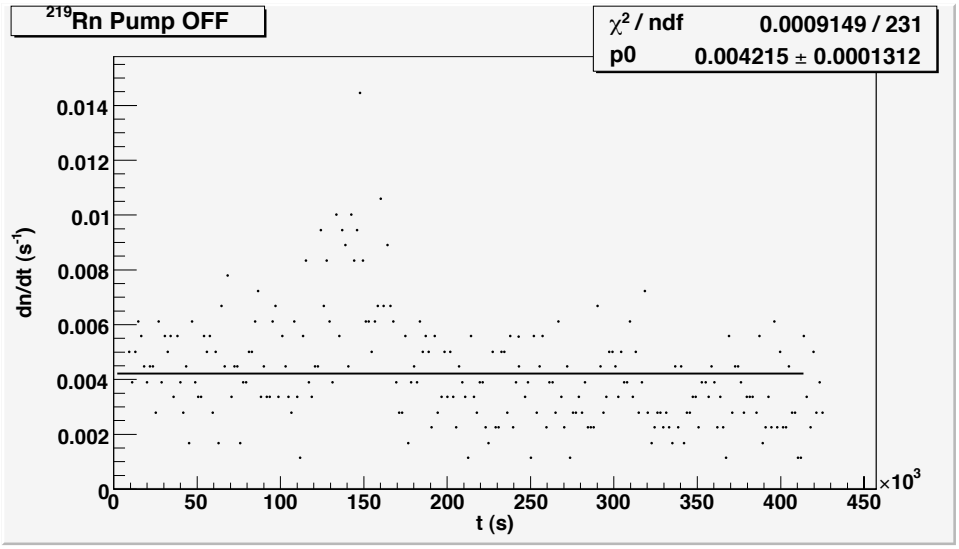


As pointed out before, the pump sucking does not affect $^{219}Rn$ activity, and we have obtained very similar values from the fit results, both very close to $4 \cdot 10^{-3}$ counts/s.

# 7 Scattering Rutherford

Rutherford scattering represents the effect of the coulombian interaction between target nuclei and $\alpha$ particles. In order to get a good interaction rate a $^{79}Au$ layer is used. Two circular holes shield the $^{241}Am$, one placed directly on the source and the second one at the height of $1,8$ cm from the source, this way the beam is collimated and accidental counts that are not due to scattering are avoided. The thin gold layer is deposed behind the hole. The $900mm^2$ detector is used for a geometric reason.

## 7.1 Gold layer thickness evaluation

In Rutherford scattering we need to know the number of target nucei. To get such information, we have evaluated the thickness of the gold layer. A direct measure is not possible, but the energy lost by particles passing through the layer is related to thickness in a simple way[5]:

$$d = \frac{\Delta E}{\rho_{Au} dE/dx} = \frac{0,288 MeV}{19,3 g/cm^3 \cdot 2,227 \cdot 10^2 MeV/g \cdot cm^2} = 6,7 \cdot 10^{-5} cm$$

## 7.2 Rutherford Scattering

We are interested in the relation between counting rate and scattering angle. On the detector is placed a mask that leaves as active area only an outer circle of 1.1 cm radius

[5]the value for $\frac{dE}{d\rho x} = 2,227 \cdot 10^2 Mev/g\,cm^2$ for the gold is taken from http://physics.nist.gov/PhysRefData/Star/Text/ASTAR.html

and 0.12 cm width. Varying the scattering angle is possible by changin the source-detector distance from 2.2cm to 1 cm by 0.4 cm steps.

Counting rate $\frac{dN}{dt}$ is given by the area under the peaks in the detected spectra divided by measure duration. The error on angle evaluation is small compared to the error on counts. The relatively small amount of statistic leads to a low accuracy in rate esteem, due to the fact that peaks are not well defined.

Data are fitted with the function

$$\frac{dN}{dt} = \frac{p_0 sin\theta}{(sin\frac{\theta}{2})^{p_1}} d\theta$$

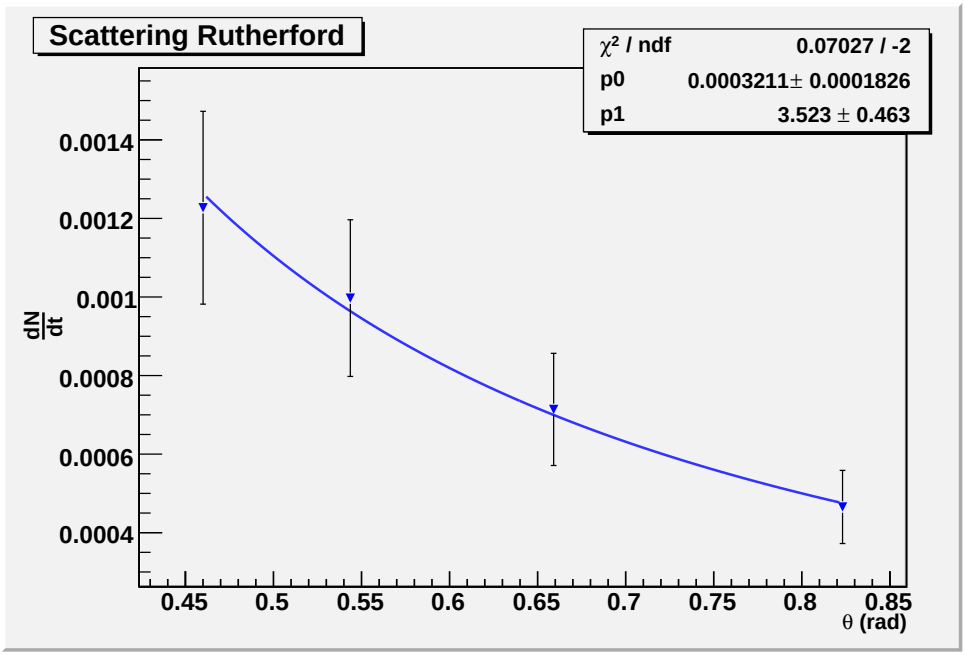


We expect this relation between rate and angle

$$\Delta R = R_0 N_A \frac{\rho A d}{A} k^2 \frac{e^4}{4E_{\alpha,0}^2} z^2 Z^2 2\pi \frac{sin\theta}{(sin\frac{\theta}{2})^4} \Delta\theta$$

The free parameters $p_0$ and $p_1$ are respectively the constant and the sine exponent . The expected value are

$$p_0 = 1,7055 \cdot 10^{-3} \qquad p_1 = 4$$

Although we are not satisfied by the quantitative results of the experience, the data clearly show the expected qualitative results.